GRANJON PRIZE COMPETITION 2008
Joint Winner – Category A:
"Joining and Fabrication Technology"

CHARACTERIZATION AND OPTIMIZATION OF ORBITAL FRICTION WELDING OF HIGH CARBON STEEL BARS

M. Maalekian

ABSTRACT

The purpose of the present paper is to characterize and optimize the orbital friction welding (FW) parameters which lead to a sound joint quality of eutectoid steel bars. To optimize the weld microstructure, the phase transformations taking place in the FW of eutectoid steel is studied and the influence of peak temperature and plastic deformation of austenite on the continuous transformation behaviour are investigated. It is also demonstrated that modelling of FW depends entirely on the frictional heat flow term, which can be estimated with an inverse heat transfer analysis. By developing 3-D finite element models based on the estimated frictional heat, the temperature profile, axial shortening, flash formation, microstructure evolution during FW and the size of the heat-affected zone are effectively studied.

IIW-Thesaurus keywords: *Austenite; Computation; Finite element analysis; Friction welding; Martensite; Orbital friction welding; Pearlite; Phase diagrams; Reference lists.*

1 INTRODUCTION

Friction welding (FW) is a solid-state joining process in which the frictional heat is generated by the relative movement of two components under friction force. Once sufficient heat has been generated, the rubbing action is terminated and the pressure is usually increased in the forging stage to consolidate the weld. The joint has a narrow heat-affected zone and shows plastically-deformed material, subject to severe plastic deformation due to the high local temperature and internal pressures. The FW process has recently been reviewed thoroughly [1]. Three variants of FW are widely used: rotary, linear and orbital friction welding. In rotary friction welding, one component is rotated around its axis while the other remains stationary. For welding, the two components are brought together via the application of pressure. In linear friction welding, the parts move under friction pressure relative to each other in a reciprocating fashion, through a small linear displacement (amplitude) in the plane of the joint to be made. In orbital friction welding (Figure 1), which is a combination of linear and rotational friction welding, the centre

Dr. Mehran MAALEKIAN (mehran.maalekian@ubc.ca) is formerly of the Institute for Materials Science and Welding, Graz University of Technology, Graz (Austria). He is now with the Department of Materials Engineering, The University of British Columbia, Vancouver (Canada).

Doc. IIW-1979-08 (ex-doc. III-1510r1-08) recommended for publication by Commission III “Resistance welding, solid state welding and allied joining processes”.

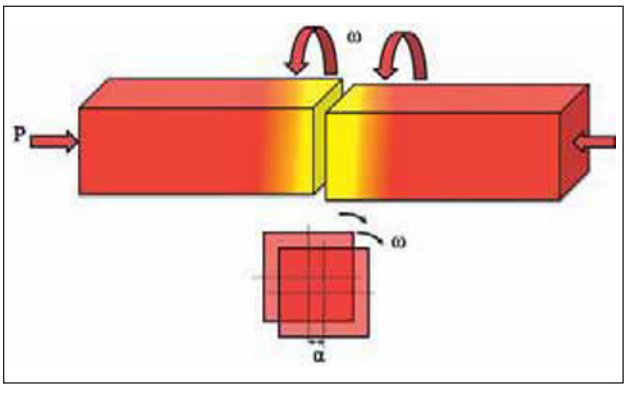

ω is the angular speed, α is the amplitude (axes offset) and P denotes the friction and forge pressure.

Figure 1 – Schematic of the orbital friction welding process

of one component relative to the other component is moved around a two-dimensional curve (e.g. a circle) to provide the rubbing action. The two parts to be joined are rotated around their longitudinal axes in the same direction and with the same constant angular speed (ω). The two longitudinal axes are parallel except for a small distance offset (α). When motion of the components ceases and before friction pressure is applied, the parts are correctly aligned to form a weld.

On comparison of the different friction welding techniques, rotary friction welding is seen to have the inherent limitation that it cannot be used for non-circular, cross-section components. Another main disadvantage is that the rate of heat generation is not uniform over the interface. This gives rise to a non-uniform thickness of the heat-affected zone. These shortcomings can be avoided by using linear or orbital friction welding. The two methods can be used for the welding of non-circular parts and the interfacial energy generated is almost uniform. The frictional heat generation at the interface of two components for the orbital, as compared to the linear, method, is even more uniform, attributed to the unvarying, unidirectional, relative velocity between the two components over the total interface area [2].

In orbital friction welding, four parameters control the character of the weld, through determination of the amount of energy input to the weld and the rate of heat generation at the interface: the relative velocity between the workpieces, the duration of the process, the axial force and the amplitude. Due to the direct conversion of mechanical to thermal energy at the mating surfaces, friction welding is inherently rapid and economical. In present times, friction welding has found widespread industrial applications and is used widely as a reliable and automated process. For example, the problems encountered in the fusion welding of high carbon steel (e.g. eutectoid steel) due to its poor weldability, can also be overcome by using the FW process.

It is important to understand the concept of the process and to know how the change in process parameters can influence the joint properties. Such an understanding will help to improve the weld quality, to eliminate weld defects and to transfer knowledge of the welding procedure to new conditions (e.g. for new geometry or new material). Therefore, modelling of the process, with the aim of predicting the weld properties as a function of process parameters, has been a central part of the investigation of friction welding processes for several decades [1]. Since the late 1950s, the process has been widely studied both analytically and numerically [3-20]. Empirical and analytical studies, as well as computer-based models of the friction welding (FW) process, have been developed to examine heat flow, material deformation, microstructure evolution and solid-state phase changes. Although the investigations have been very useful towards the understanding of the different physical, metallurgical and mechanical aspects in friction welding, most of the models are insufficient due to the lack of an accurate expression for the heat generation term [1]. Several phenomena associated with the process, such as severe plastic deformation, steep temperature gradients, very high rubbing velocity and strain rate and their influences on the frictional behaviour of the material and solid-state phase transformations, make analyses of the FW very difficult. Another difficulty is the understanding of the dependency of the friction coefficient on temperature, pressure and velocity.

Orbital friction welding, compared with the other types of friction welding (i.e. linear and rotary), has been investigated very insignificantly. The reason can be attributed to the relative complexity of the process machinery of orbital friction welding. There is very limited work published on the orbital FW process and, to the author's knowledge, no experimental data has yet been published. Though there is a wealth of information on the other types of FW processes (particularly rotary FW), mostly gathered empirically, many factors such as specimen geometry, surface conditions, material properties and type of relative movement (e.g. linear and rotational) can significantly influence the welding process and for different materials or processes, each of the optimized parameters is different.

The aim of this work is to characterize and optimize the orbital friction welding parameters which lead to a sound joint quality of eutectoid steel bars. To optimize the phase transformations taking place in friction welding of eutectoid steel, the influence of FW temperature and the straining of austenite on the kinetics of austenite decomposition in continuous cooling cycles are studied. This will help to optimize the pre- and/or post-weld heat treatment in order to achieve acceptable microstructure, hardness and weld toughness. For the numerical modelling of the FW process, a recent approach based on the inverse heat transfer method for modelling the heat source is used [17]. Unlike most analytical approaches, this method is not based on a high degree of knowledge about the frictional and plastic deformation behaviours of the material at a wide temperature range (from low temperature to the solidus temperature) [20]. Based on the inverse analysis data and using a 3-D, coupled, thermo-mechanical, finite element (FE) model, the temperature profile, axial shortening and flash formation at the joint interface are

predicted. In a coupled, thermal-phase transformation FE model, the microstructure evolution and the final microstructure of the weld and the size of the HAZ are effectively investigated.

2 FRICTION WELDING EXPERIMENT

The chemical composition of the steel studied is 0.75C, 1.02Mn, 0.28Si, 0.11Cr, 0.05Ni, 0.015S, 0.009P, 0.08Cu (wt-%). The steel has a fully pearlitic microstructure (Figure 2). A novel orbital friction welding machine was used to produce a weld between steel bars of various dimensions, e.g., 88 × 20 mm (Figure 3). A PC-based data acquisition system was designed to monitor and record axial displacement, rotation speed and axial force during welding. The temperature changes during the friction welding process were measured by thermocouples attached to the steel bar at distances of 2.5, 5.0 and 7.5 mm from the rubbing surface and 4 mm deep into the bar. Figure 3 shows the appearance of a welded specimen and the initial thermocouple positions.

As previously pointed out, due to the very limited work and data published on the orbital FW process, in order to achieve a sound weld in the present work, the orbital FW parameters were obtained empirically. At the beginning of this work, various combinations of the FW parameters were tested, but all of the trials were unsuccessful and not a single sound weld was obtained. The influence of contact surface quality was also investigated by using a very smooth rubbing surface. However, it was experimentally observed that the surface quality (i.e. roughness/smoothness) of the faying surfaces is not noticeable. This result is also supported by Vill's investigations [4] on the rotary friction welding of mild steel.

Figure 2 – Fully pearlitic microstructure of the base material (eutectoid steel)

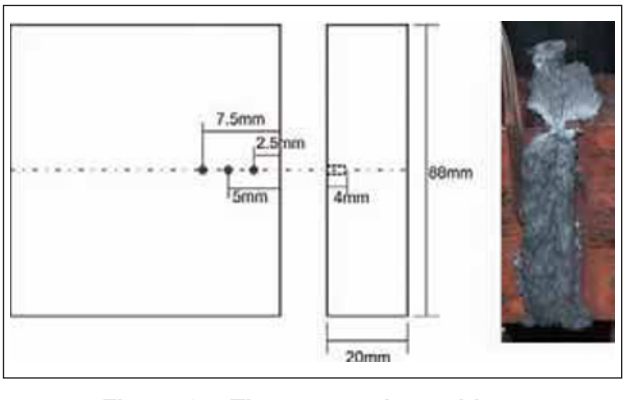

Figure 3 – Thermocouple positions and the friction-welded specimen

For further investigation, the relative motion of the two parts in the course of friction welding was also analyzed by a high-speed camera recording 125 images per second. The recorded images were analyzed with the image analyzer software, ZEISS-KS400. The results showed that the relative motion of the two parts was not sustained during the entire welding cycle. As shown in Figure 4, after a short period of time, the relative movement of the two components is reduced to zero from the prescribed offset distance (amplitude). In other words, the two parts were moving synchronously instead of moving against each other. The reason is attributed to the formation of metallic junctions on the friction surface. These regions, as soon as they form, should be broken down rapidly. However, due to the insufficient frictional heat produced with the preliminary process parameters, the destruction of the seized regions is impossible and only a small region of the faying surface is welded. Therefore, by using this methodology and increasing the dissipated heat at the rubbing surface, proper welding parameters could be obtained. Further details of the experimental procedure and the acquired optimum process parameters are provided in [2]. For example, Figure 5 shows the required friction and forge forces at a specified amplitude and velocity for the orbital FW of the specimens illustrated in Figure 3.

The microstructure of the friction-welded rectangular bars is shown in Figure 6. As expected for eutectoid steel with high carbon content, in the central weld region (close to the weld line) the microstructure is

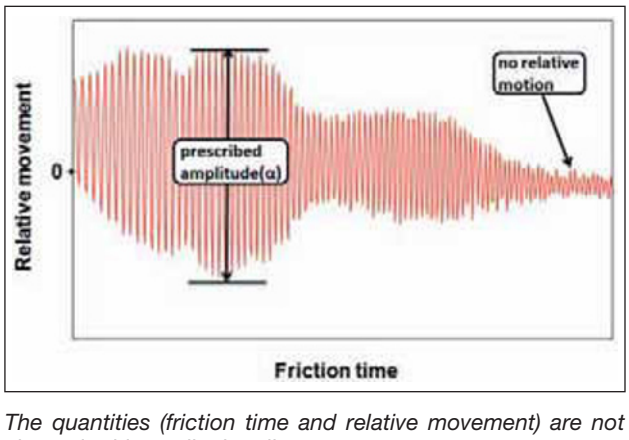

The quantities (friction time and relative movement) are not shown in this qualitative diagram.

Figure 4 – The relative motion of the two parts at prescribed offset distance (α) and other FW parameters, recorded by a high-speed camera and quantified by an image analyzer

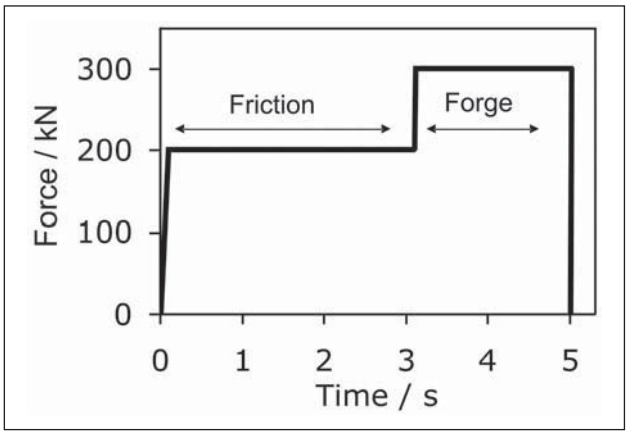

Figure 5 – Friction and forge forces and friction time (at specified amplitude and velocity) used for the orbital friction welding of the specimens shown in Figure 3

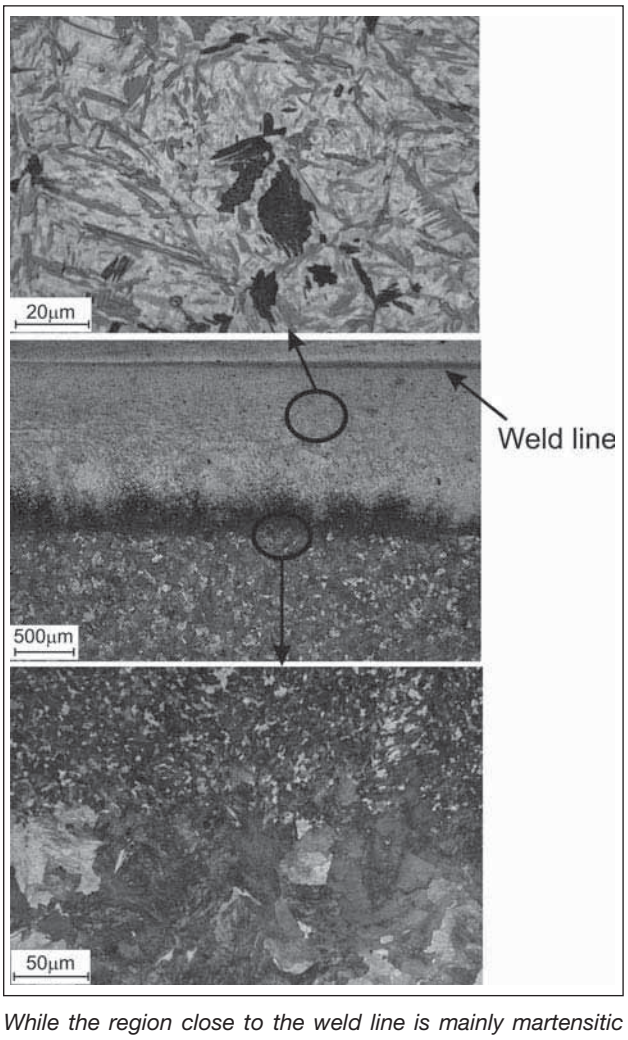

While the region close to the weld line is mainly martensitic (upper picture), the microstructure changes to fine pearlite with a low amount of martensite (lower picture) when moving towards the base metal (i.e., coarse pearlite).

Figure 6 – Microstructure of eutectoid steel orbital friction weld, HAZ and base metal

mainly martensitic, with minor pearlite and bainite volume fraction. It is also revealed that a fine pearlitic microstructure is formed in the HAZ close to the base metal which consists of coarse pearlite. When compared to the parent metal (Figure 2), in the weld region, the initial coarse pearlite microstructure is transformed into mainly martensite, with small amounts of bainite and fine pearlite. The reason for the martensitic phase transformation at the weld centre, as will be shown later on the present paper, is the intensive heat input during orbital friction welding and the steep temperature gradient.

It is desirable to be able to predict weld shape (flash formation), as a function of the FW process parameters, and to understand the influence that changes in these process parameters may have on the final weld profile. By a neural network analysis, the influence of friction welding parameters on the flash formation has been investigated [2]. The experimental data obtained have been used to describe the integrity of the weld in terms of the weld-collar. Inputs to the network are the friction welding parameters, namely amplitude, friction force, friction time and rotation speed. The prediction of the influence of welding parameters on the quality of the weld, in terms of the size of the flash, has been studied. Details of the neural network analysis can be found elsewhere [2, 21].

3 PHASE TRANSFORMATION IN THE FW OF EUTECTOID STEEL

During the friction welding process, the steel part is subjected to high pressures leading to macroscopic deformation of the specimens, in addition to the high temperature gradients. The accompanying phase transformations then occur under simultaneous stress and plastic deformation and the effect of plastic deformation must be taken into consideration. Consequently, phase transformations occurring during this solid state welding operation differ markedly from those which occur during conventional heat treatment and thermo-mechanical processing. However, according to the author's knowledge, little or no effort has been made to investigate the influence of severe prior austenite deformation on the austenite decomposition, under fast heating and cooling conditions typical of the FW welding processes. Hence, to obtain greater understanding of the phase transformations taking place in eutectoid steel, the aim of this part is to assess the influence of peak temperature and plastic deformation of austenite on the onset of phase transformations in continuous cooling cycles.

3.1 Thermal and thermo-mechanical cycles

Continuous cooling transformation (CCT) diagrams provide a comprehensive picture of the austenite transformation kinetics. However, application of CCTs to accurately describe the transformation behaviour in weldments is critical, since weld thermal cycles are very different from those used for generating conventional CCT diagrams. Therefore, construction of welding continuous cooling transformation diagrams

(WCCT) of unstrained and strained austenite makes it possible to draw valuable conclusions about the deformation effects on phase transformation taking place in the FW process. The WCCT diagram for undeformed and deformed conditions is constructed based on the microstructural characterization, dilatometry, hardness and microhardness data.

Physical simulation of the weld thermal and thermo-mechanical cycles was performed on a *Gleeble-1500* testing machine. Specimens used for experiments were machined into cylinders of 12 mm diameter and 110 mm length (Figure 7). According to the temperature measurements during the friction welding experiment at different distances from the weld line, two austenitizing temperatures, 1 300 and 1 100 °C, were chosen. The thermal and thermo-mechanical cycles, as well as the schematic of the samples, are shown in Figure 7.

During the thermal cycle, the specimens were heated at 100 Ks^{-1} to the peak temperature (1 300 or 1 100 °C) and maintained there for one second, before allowing them to cool. In the thermo-mechanical case, the samples were deformed by compression in a longitudinal direction, within the range 1 000-900 °C at constant load 13 kN, the strain being implemented within 3 s. They were then cooled while monitoring the change in diameter. All experiments were carried out in an argon atmosphere. A combination of microscopy, dilatometric analysis, Vickers hardness and microhardness analysis was used to determine phase transformation temperatures, microstructure evolution and mechanical properties. Following thermal or thermo-mechanical treatment, the samples were ground, polished and etched in 3 % Nital solution. Metallographic examination was conducted on the centre region of the central cross-section normal to the compressive axis of specimens, as shown in Figure 7.

3.2 Effect of peak temperature on the welding CCT diagram

The influence of the peak temperature on the WCCT diagram is shown in Figure 8. The higher austenitizing temperature shifts the diagram to longer times, i.e. hardenability is increased. This effect can be attributed to grain coarsening and homogenization phenomena. Figure 9 depicts the influence of peak temperature on austenite grain size, which has been revealed by optical microscopy in fast cooling rate condition ($t_{8/5}$ = 5-6 s), where final microstructures are fully martensitic. The images have been manually reconstructed from the optical micrographs using the image analyzer software ZEISS-KS 400. It illustrates that the austenite grain size in the 1 300 °C peak temperature cycle is much coarser than that of the 1 100 °C cycle. The austenite grain size prior to cooling has substantial influence on the hardenability of steels. Austenite grain boundaries act

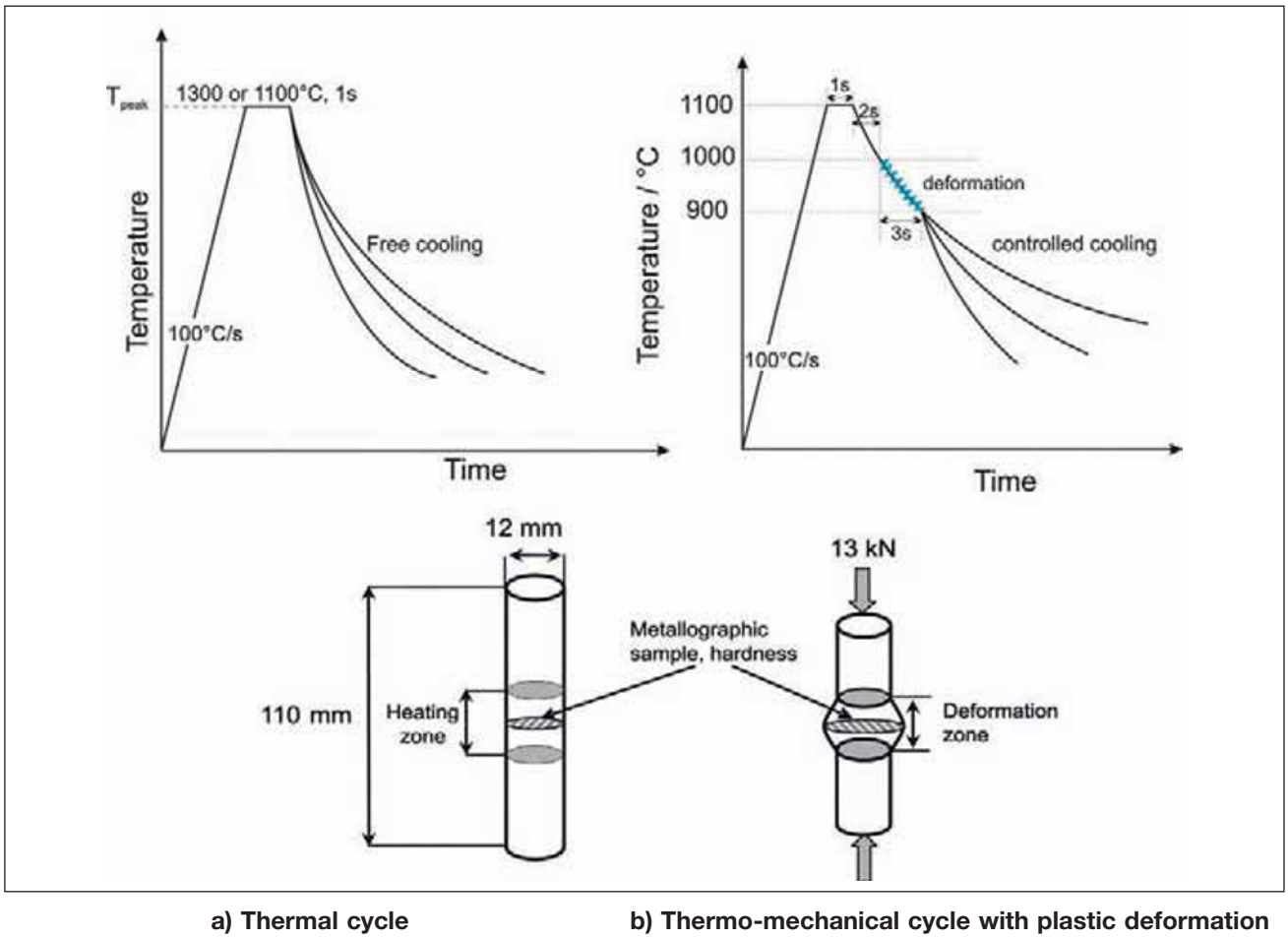

a) Thermal cycle

b) Thermo-mechanical cycle with plastic deformation of austenite prior to transformation

Figure 7 – Schematic illustration of the thermal and thermo-mechanical cycles and of the specimens used

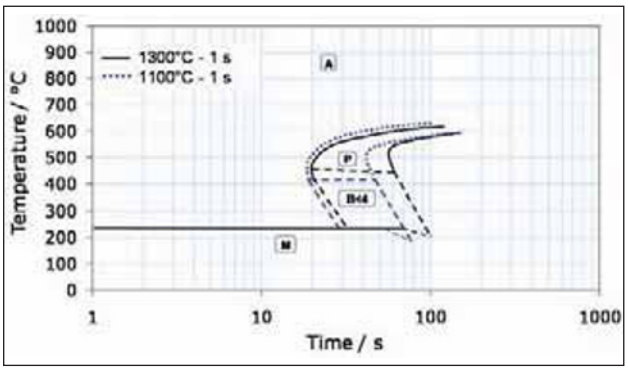

A: austenite; B: bainite; P: pearlite and M: martensite. The bainite region is indicated with a dashed line because the start and end points could not be clearly identified by dilatometry due to the low quantity of bainite (< 4 %). However, this line was revealed by microstructure and microhardness analyses.

Figure 8 – The influence of peak temperature on the welding CCT diagram

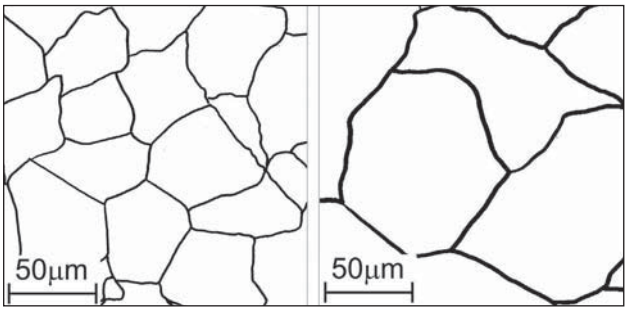

T_{peak} for the image on the left is 1 100 °C, while it is 1 300 °C for the image on the right.

Figure 9 – Prior austenite grain size revealed by optical micrograph and image analyzer in fast cooling rate conditions ($t_{8/5}$ = 5-6 s) with fully martensitic microstructure

as heterogeneous nucleation sites for the formation of non-martensitic transformation products. Therefore, with larger grain boundary area, i.e. smaller grain size, reconstructive transformations are taking place at a faster rate.

Moreover, it should be pointed out that the rate of heating and the holding time during the thermal or thermo-mechanical cycle have profound influence on austenite homogenization (carbide dissolution) and the hardness after cooling. The time-temperature-austenitizing diagram (continuous heating) for a similar steel [22] (see Figure 10) verifies that full homogenization is achieved under the present experimental conditions. Consequently, the shift in the WCCT diagram can be attributed to the austenite grain size.

3.3 Effect of austenite deformation on the welding CCT diagram

The influence of hot compressive deformation of austenite on its continuous decomposition, carried out

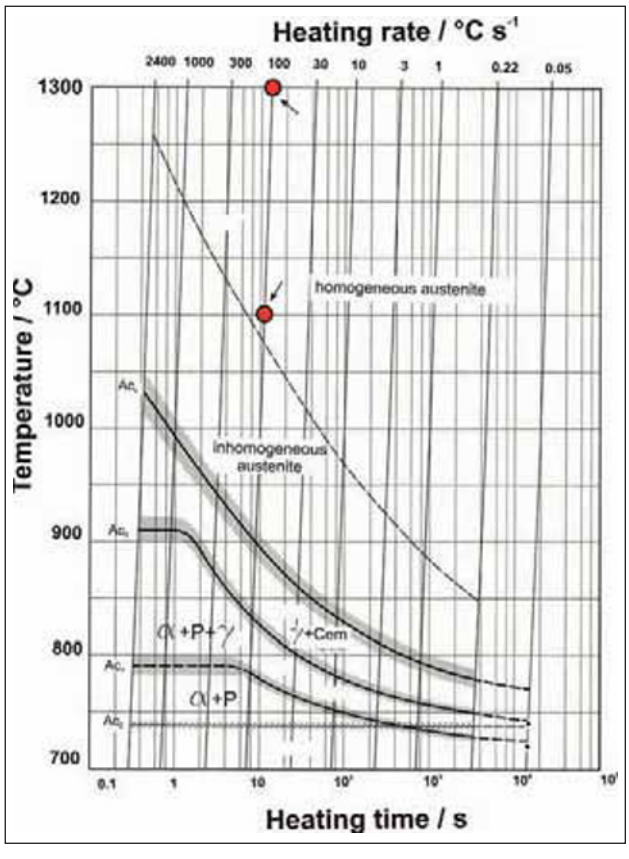

The two red points indicate the austenitization conditions for the two peak temperatures at the end of the heating cycle.

Figure 10 – Continuous time-temperature austenitization diagram for the steel C 70 W 2 with a similar chemical composition to the eutectoid steel studied [22]

in a temperature range of 1 000–900 °C, is shown in Figure 11. Severe plastic deformation of austenite to the effective strain of $\varepsilon \approx 0.4$-0.9 accelerates the reconstructive (here pearlite) transformation, which shifts its existence region in the WCCT diagram to higher cooling rates and raises start-finish temperatures. Simultaneously, the martensite start temperature is lowered slightly which is attributed to the mechanical stabilization phenomena [23-24] and will be discussed in the following sections. The reason for these two contradictory observations, that pearlite is accelerated but martensite is retarded when transformation occurs from plastically-deformed austenite, lies in the different mechanisms of phase change for pearlite and martensite.

Figure 11 also shows that, at low cooling rates, the acceleration of the pearlite transformation is lower or almost negligible. It reveals that the degree of acceleration depends on the cooling rate. In continuous cooling at high temperatures, there is a post-deformation delay, which is the time interval from the moment of deformation completion until the start of austenite decomposition. At low cooling rates, particularly when the deformation temperature is high, in the range of 1 000-900 °C, static recrystallization and grain growth can take place [25-28]. The lower the cooling rate, the smaller the extent of transformation acceleration for deformed austenite. Then, due to the longer post-

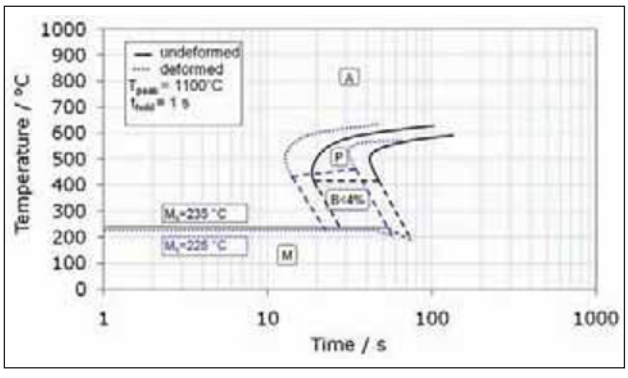

Figure 11 – The influence of hot compressive deformation of austenite on the WCCT diagram

deformation delay, the state of the deformed austenite becomes similar to the undeformed one. Under these circumstances, the pearlite ranges for deformed and undeformed steel coincide in the WCCT diagram [29].

When the material undergoes recrystallization, either during or after hot deformation, the austenite grain size decreases. Therefore, the increase in the transformation rate can be attributed to the rise in the austenite grain surface area (see [27-28]). The deformation temperature and strain rate in the present thermo-mechanical treatment are 1 000-900 °C and 0.1-0.3 s^{-1}, respectively. Under these circumstances, within a few seconds, partial recrystallization takes place, as reported in [30] for a high carbon tool steel with similar chemical composition to the present steel. The decreasing grain size for deformed austenite indicates that recrystallization takes place during (dynamically) or immediately after heavy deformation. Due to the increasing heterogeneous nucleation site density, the pearlite transformation takes place at shorter times and higher temperatures, in comparison with austenite decomposition without plastic deformation [28].

3.4 Mechanical stabilization

In the WCCT diagram (Figure 11), it is illustrated that the martensite-start temperature M_s of the deformed austenite is depressed by ~10 °C, compared to the undeformed austenite. This observation should, in principle, be explained by the theory of mechanical stabilization [23].

Displacive transformations, such as the martensite transformation, involve the coordinated movement of atoms. Such movements cannot be sustained against strong defects such as grain boundaries [24]. Thus, martensite plates do not traverse austenite grain boundaries. Defects such as dislocations also hinder the translation of the martensite-austenite interface. It has been known for some time that the plastic deformation of austenite before its transformation retards the growth of martensite, a phenomenon known as mechanical stabilization. This can be explained quantitatively by balancing the force driving the transformation interface against the resistance from dislocation debris in the austenite [24].

The theory for mechanical stabilization relies on balancing the force required to move austenite/martensite interface through a forest of dislocations, against the force owing to the chemical-free energy change ($\Delta G^{\gamma\alpha}$) driving the interface:

$$\frac{Gb\rho^{\frac{1}{2}}}{8\pi(1-\upsilon)} = \left|\Delta G^{\gamma\alpha}\right| \quad (1)$$

where

b is the magnitude of the Burgers vector,

G is the shear modulus of the austenite,

υ is its Poisson's ratio and

ρ is the dislocation density.

$\Delta G^{\gamma\alpha}$ for transformation without a composition change was calculated using MT-DATA [31] as shown in Figure 12.

The deformed and undeformed samples transform at different temperatures, i.e. at different driving forces, so that:

$$\Delta(\Delta G^{\gamma\alpha}) = \Delta G^{\gamma\alpha}_{235°C} - \Delta G^{\gamma\alpha}_{225°C} = 70 \ \text{Jmol}^{-1}$$

where

$\Delta(\Delta G^{\gamma\alpha})$ is the magnitude of the change in available driving force due to the presence of dislocation in austenite

Using Equation (1) and Figure 12, the following equation can be obtained [23]

$$\frac{\mu b}{8\pi(1-\upsilon)}(\rho^{\frac{1}{2}} - \rho_0^{\frac{1}{2}}) = \Delta G^{\gamma\alpha}_{M_s} - \Delta G^{\gamma\alpha}_{M_{s0}} = \Delta(\Delta G^{\gamma\alpha}) = 7.0337\Delta T \quad (2)$$

where

ΔT is the reduction in M_s temperature due to deformation and

M_{s0} is the martensite-start temperature in the absence of deformation and

ρ_0 is the dislocation density at zero plastic strain.

The theory calculates the depression of transformation temperature M_s as a function of the change in the dislocation density of the austenite.

The predicted depression in the martensite-start temperature according to the mechanical stabilization

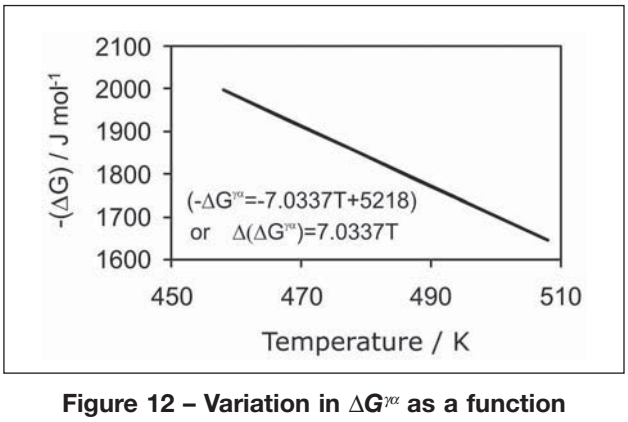

Figure 12 – Variation in $\Delta G^{\gamma\alpha}$ as a function of temperature for the pearlitic steel studied

theory is shown in Figure 13. The calculated values compare well with the measured value.

4 CALCULATION OF FRICTIONAL HEAT FLOW

In friction welding, the temperature in the weld region rises sharply due to friction and plastic work. In all thermal models of FW, the main task is to calculate the temperature profile in the specimen by solving the heat transfer equation. To calculate the temperature profile, the heat transfer analysis is undertaken by considering the frictional heat generation at the interface, heat generation by plastic deformation and heat loss to the environment. For the homogeneous and isotropic continuum with temperature-dependent material characteristics, the following equation of heat conduction applies, which is based on the principle of conservation of energy:

$$\rho C_P \frac{\partial T}{\partial t} = \frac{\partial}{\partial x_i}\left(k \frac{\partial T}{\partial x_i}\right) + \rho C_P u \frac{\partial T}{\partial x_1} + \dot{S} \quad (3)$$

where

ρ is the material density,

C_P is the specific heat,

k is the thermal conductivity,

T is the temperature,

t is the time and

x_i with index notation of i=1, 2 and 3 represents x, y and z directions, respectively.

The convective term on the right hand side of the equation accounts for the shortening of the specimen during friction welding, which is given by the product of the temperature gradient and the shortening velocity u. The volumetric heat source term $\dot{S}$ (W m^{-3}) arises from plastic work in the workpiece next to the faying surface. In the present work (i.e. for the inverse analysis), for the benefit of simplicity, the heat generation from plastic dissipation ($\dot{S}$) is ignored, due to its low value compared to the frictional heat generation reported in

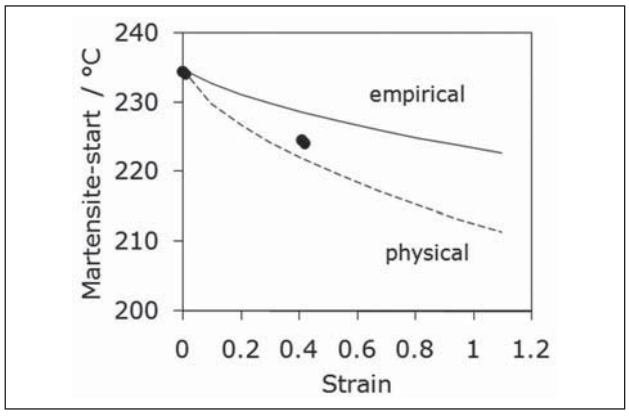

Two alternative methods used for the approximation of dislocation density [23]: the first is labelled empirical, since it relies on measurements taken on a different steel, and the second, physical, because it begins with an assumption about stored energy. The measured values are shown by filled circles.

Figure 13 – Calculated change in M_s as a function of the plastic strain in austenite prior to its transformation

[19]. Figure 14 shows the schematic views of different regions arising during FW, as well as the coordinate system and boundary conditions for a specimen with general geometry.

The major boundary condition is the frictional heat generation at the interface, taken as follows:

$$-k \frac{\partial T}{\partial x}\Big|_{x=0} = q(t) \quad (4)$$

where

$q(t)$ is the frictional heat generation at the interface.

The objective is to calculate the surface heat flux, $q(t)$.

In the FW process, the welding parameters are defined when the generated heat at the faying surface enables the material to soften and a sufficient size of weld collar is formed, by flowing plasticized material out of the abutting surface. Three main parameters control the properties of a weld: rubbing velocity (v), friction

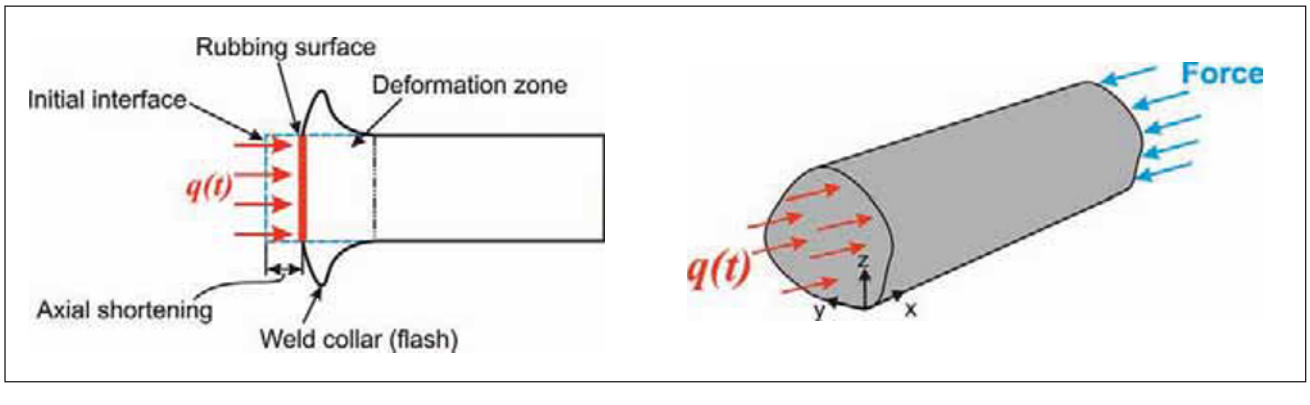

a) Schematic view of different zones arising during friction welding of a specimen

b) Coordinate system and boundary conditions used for the modelling

Figure 14

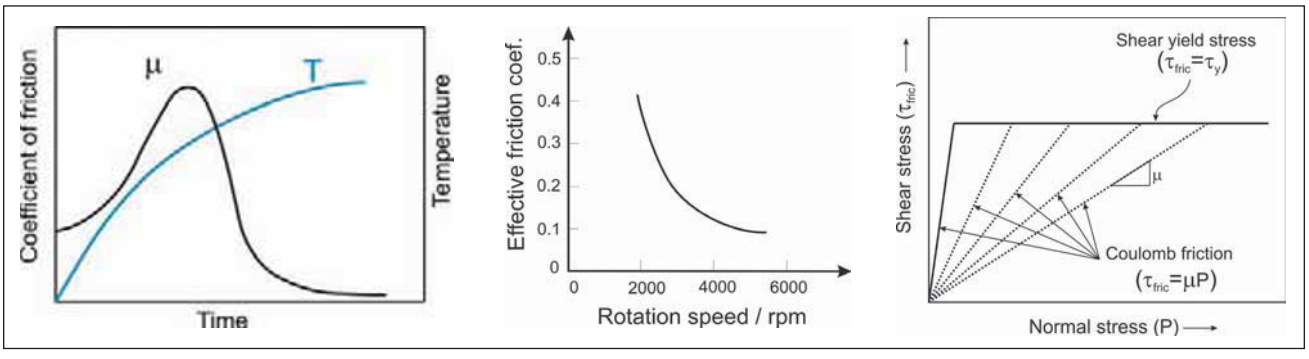

a) Variation of friction coefficient with temperature during FW of steel [32]

b) Effect of rotational speed on coefficient of friction at constant normal pressure during rotary FW of two steels [34]

c) Characterization of frictional behaviour and shear stress that resist sliding between the two surfaces

According to the Coulomb friction law, the shear stress is proportional to the normal stress with a factor (μ), when the plastic deformation at the friction surface is insignificant (i.e. at low loads). Since the friction coefficient (μ) varies during the FW process, at every moment of the process an appropriate value of μ must be adopted. When the fully plastic flow occurs due to the softening of material at the interface, the friction stress and the shear yield stress are equal and frictional shear stress can be taken as the shear yield stress of the workpiece material, which also varies with temperature and strain rate.

Figure 15 – Coefficient of friction is influenced by many parameters and varies intricately during friction welding

stress (τ_{fr}) and friction time (t). The rate of heat generation $q(t)$ at the weld interface is determined with these parameters as

$$q(t) = \tau_{fr} . v \quad (5)$$

The major unknown term in the thermal analysis of friction welding is the shear stress due to friction (τ_{fr}). It is usually assumed that the resistance to sliding along the interface between the workpieces is uniform along the entire contact surface. The most common simplifying assumption made with regard to friction stress (τ_{fr}) between the workpieces involves Coulomb friction. For Coulomb friction, it is assumed that the contact shear stress (τ_{fr}) is proportional to the contact (normal) pressure (P) with the proportionality factor (μ) called the Coulomb coefficient of friction [i.e. $\tau_{fr} = \mu P$, see Figure 15 c)].

Many factors such as temperature, surface roughness, material properties and magnitude of rubbing velocity affect frictional behaviour (μ) and the forces (τ_{fr}) that resist sliding between the two surfaces. In literature of reference, many different friction coefficient values are reported, even for the same sliding materials, which are attributed to the large number of potential friction-affecting factors. For example, Gel'man and Sander [32-33] discovered that the friction coefficient decreases with an increase in pressure and velocity and with a raise of temperature, it increases rapidly at the beginning of the FW process and then decreases, as illustrated in Figure 15 a). On the other hand, Hollaner *et al*. [34] found that the effective coefficient of friction decreases as rotational speed increases [Figure 15 b)]. However, due to the change in surface conditions (e.g. temperature, strength and roughness) at every moment of friction welding, a different friction coefficient value should be chosen, in order to adopt an appropriate shear stress on the welding interface [Figure 15 c)]. Moreover, because the Coulomb friction law is based on rigid contact surfaces, when severe plastic deformation is involved, as in friction welding, the Coulomb friction is not sufficiently representative for the frictional heat generation. Consequently, the friction coefficient is an established, but somewhat misunderstood quantity in the field of science and engineering. Therefore, it is rather impossible to find the exact coefficient of friction, particularly for friction welding processes, by consulting values in published tables of friction coefficients and any description of friction welding based only on the friction coefficient value is suspect [1].

This dilemna can be overcome by an *inverse* heat conduction (IHC) approach; which is a convenient method for the analysis of heat generation at inaccessible locations such as the friction surface. Therefore, due to the practical difficulty involved in the exact measurement of surface temperature or surface temperature gradient, the surface conditions can be estimated from temperature measurements made at some convenient positions inside the solid, see Figure 16. Such a problem

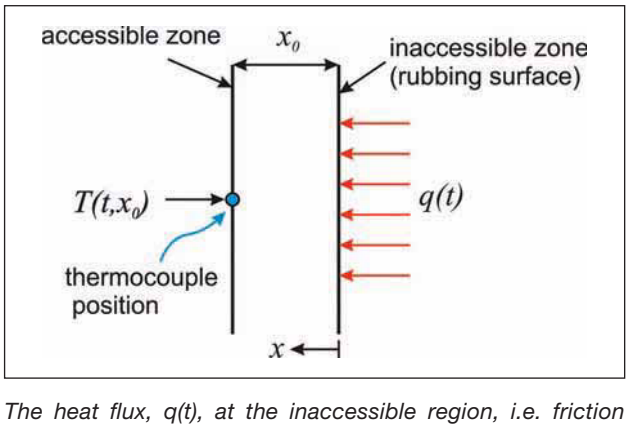

The heat flux, q(t), at the inaccessible region, i.e. friction surface, is estimated from the temperature data measured at the accessible region (i.e. at an interior location such as x_0).

Figure 16 – Schematic of inverse heat conduction method

is termed as the *inverse* problem of heat conduction, wherein the temperature history at an interior point is prescribed and the surface conditions are calculated from the solution of the transient heat conduction equation, satisfying the prescribed interior conditions [17, 19]. This is in contrast with the direct problem of heat conduction, where the boundary conditions are prescribed at the surfaces and the interior conditions are calculated.

As pointed out previously, the objective is the calculation of the surface heat flux, *q(t)*, based on the temperature measurements during the welding experiment at position ($x=x_0$, at Figure 16). The inverse problem is solved by minimizing the objective function, *R*, which is the least square norm defined as:

$$R = \sum_{j=1}^{J} \sum_{i=1}^{I} (Y_{ij} - T_{ij})^2 \qquad (6)$$

where

Y_{ij} and T_{ij} are the vectors containing the measured and predicted temperatures and the superscripts *i* and *j* indicate distance and time increments, respectively.

The details of the inverse approach can be found elsewhere [17, 19].

For the analysis of FW, heat generation and pressure across the interface are assumed to be uniform. The uniformity of interfacial heat generation in the orbital friction welding was experimentally verified by the observation of a uniform width of the HAZ reported in [2, 18]. Moreover, this assumption was also mathematically confirmed for small values of the amplitude [35]. Uniform pressure is also a general assumption, frequently used by many researchers in modelling FW for many decades (e.g. [9, 36-37]). Furthermore, since the duration of the friction welding cycle is very short, i.e. typically, a few seconds, the radiation and convection heat losses are insignificant. Therefore, in the inverse model, the lateral surfaces of the specimen are assumed to have an adiabatic boundary condition and the temperature distribution which exists across the plane parallel to rubbing surface is uniform [19].

The calculated heat generation at the friction interface, using the IHC method for the orbital friction welding of eutectoid steel bars, is shown in Figure 17. The welding conditions and the thermo-physical properties are given in [19]. For the thermal modelling of FW, unlike the approach based on friction theory and shear work (i.e. Equation (5) and Figure 15), the inverse heat conduction approach does not require as much information such as surface temperature, shear yield stress and friction coefficient. The main requirement for the inverse approach is the temperature data, measured at a location near to the friction-heated region.

A measure of how well the proposed models represent the actual heat generation rate can be deduced by comparison of the predicted and measured temperature data. For the purposes of comparison, the calculation based on the friction theory (sliding and sticking [20]) is also included. The computed temperature profiles at the position of x_0 = 2.5 mm (the initial distance from the interface) are shown in Figure 18 and compared with the actual data. The heat generation obtained from the IHC method predicts the temperature profile accurately, whereas prediction of friction theory is generally not promising. The poor correlation between the temperature profiles predicted by friction theory and the experimental data reveals that the friction coefficient varies significantly during the FW process, therefore the use of a constant value would lead to inaccurate results.

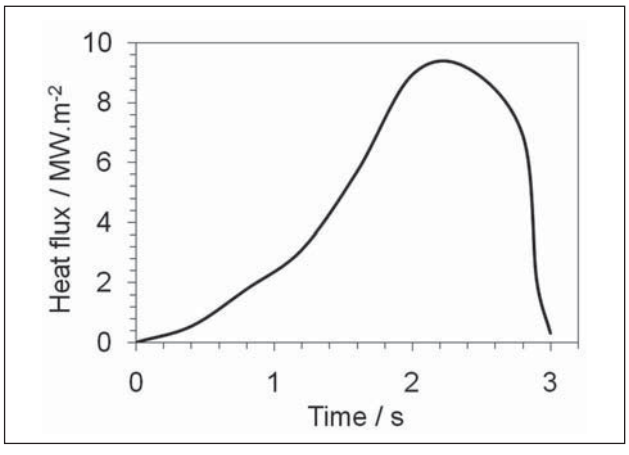

Figure 17 – Frictional heat flux at the rubbing interface, calculated with the inverse heat conduction approach for orbital friction welding of eutectoid steel

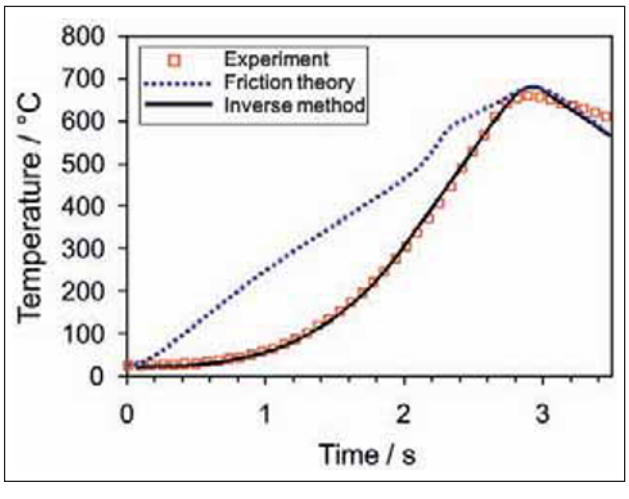

While the IHC method predicts the temperature profile accurately, the calculated temperature using friction theory is in poor correlation with experimental data. In the friction theory calculation, sliding (μ = 0.2) and sticking (full plasticity) conditions were considered.

Figure 18 – Predicted and measured temperature profiles at an initial distance of x_0 = 2.5 mm from the weld interface

5 FINITE ELEMENT MODELLING

In order to study the thermal history, flash formation and axial shortening during the orbital friction welding of eutectoid steel bars, a 3-D coupled thermal-mechanical finite element (FE) model, based on the frictional

heat generation calculated with the inverse method, is developed. Moreover, a coupled thermal-phase transformation FE model is developed to predict the microstructure evolution during the FW process in the weld and heat-affected zones. The accuracy of the FE models will also be assessed with the experimentally measured data. The FE models are developed using the commercial FE package DEFORM [38].

5.1 Thermo-mechanical model

Friction welding is, in many aspects, comparable to metal forming processes, since the material undergoes large deformation in the weld region. These processes also lead to a change in geometry and boundary conditions associated with the heat transfer problem. The process must, therefore, be modelled as a coupled thermo-mechanical problem.

In all thermal models of FW, the main task is the calculation of the temperature profile in the specimen with the solution of the heat transfer equation. Based on the principle of conservation of energy, the equation of heat conduction [Equation (3)] is undertaken with an appropriate set of initial and boundary conditions:

The volumetric heat source term $\dot{S}$ (W m^{-3}), which was ignored previously in the inverse analysis of frictional heat, is taken into account which is expressed as:

$$\dot{S} = \alpha \bar{\sigma} \dot{\bar{\varepsilon}} \quad (7)$$

where

$\bar{\sigma}$ is the effective stress,

$\dot{\bar{\varepsilon}}$ is the effective strain rate and

α is the thermal efficiency of plastic deformation, which is assumed to be 90 % [39].

The rest of this energy is principally stored as dislocations and vacancies.

Figure 19 shows the schematic view of the coordinate system and the boundary conditions, which apply to the present coupled thermo-mechanical problem. For the major boundary condition, i.e. *q(t)*, the calculated frictional heat generation by the IHC method shown in Figure 17 is employed. The convection and radiation heat transfer to the environment and the friction pressure boundary conditions are illustrated in Figure 19. For the analysis, the emissivity is assumed to be 0.7 and the convection coefficient of the environment to be 20 Wm^{-2}K^{-1}. Since a large deformation and high temperature gradients occur in the rubbing surface and the HAZ, small mesh size is used in the weld zone to improve the accuracy of the FE simulation. Due to the symmetry of the problem, only a quarter section of one of the two rectangular bars must be taken into account in the model. Heat input is defined at the right end of the bar, the thrust (friction and forge) load is applied on the left end.

5.1.1 Axial upset and flash formation

The integrity of the weld is usually determined by the size of the flash and the axial upset value. When the flash size is large enough, the hot plasticized material is expelled from the faying surfaces, carrying with it any oxides and contaminations at the interface. In this sense, the upset size (or the size of the flash) is the most important factor related to the weld quality. With the thermo-mechanical FE model, the deformation and the shape of the flash and axial shortening (upset) are analyzed.

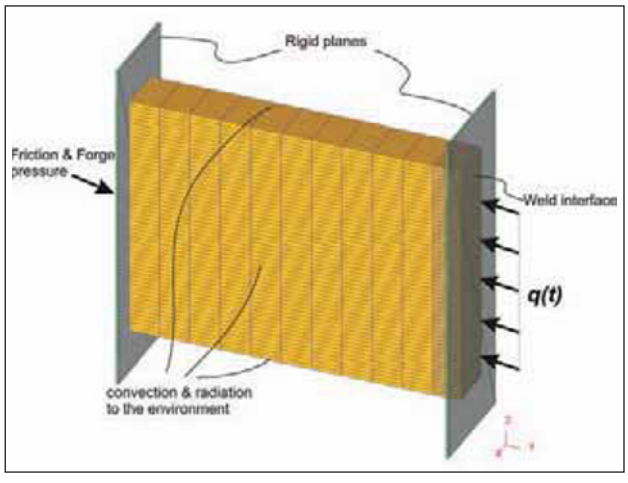

A rigid plane at the friction surface (right) is used to represent the contact area to the second bar. The other rigid plane (left) is utilized to apply friction and force pressure.

Figure 19 – Schematic view of the bar model and boundary conditions used in the thermo-mechanical FE simulation

Figure 20 schematically illustrates the shape of the flash formed during friction welding of rectangular bars and compared with the experimental observation. It shows severe plastic deformation at the weld interface, which has already been previously emphasized.

When the material at the welding joint is sufficiently softened, axial shortening is initiated and the plasticized material is expelled into the flash. Figure 21 compares the predicted axial shortening with the experiment. The experimental upset occurs mainly at the late stages of the friction welding process, whereas the predicted upset falls mostly into the forging stage (see Figure 5). This deviation in the time intervals of the upset between the FE model and the experiment is attributed to the static nature of the model. In the friction welding process, at each point of the friction phase, the plasticized material is expelled from the faying surface, due to the mutual movement of the mating surfaces, whereas the FE model is based on the static analysis in which the upset is only dependent on the thrust load and temperature. Therefore, the rubbing of the two parts, which is the main reason for the ejection of softened material from the rubbing surface, is not considered in the FE model [18]. However, apart from the difference in the starting point of the main upset between experiment and model (Figure 21), the overall upset is well-predicted by the FE model. The difference between the predicted and measured total axial shortening is only 15 %, which indicates that the model can be reasonably well applied for a prediction of the weld integrity and also for the final shape of the flash.

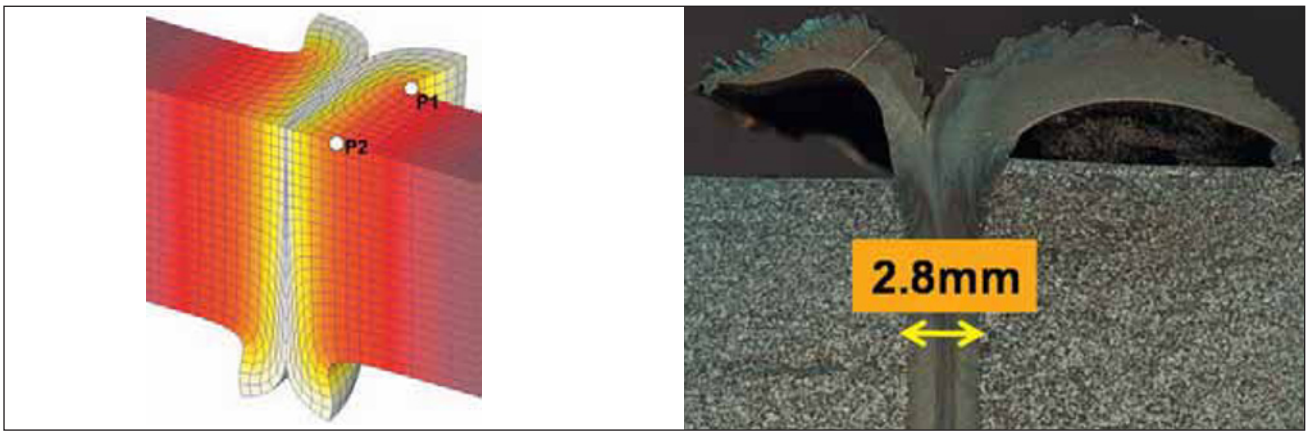

a) Schematic shape of the flash calculated with the FE model for the orbital friction welding of the steel bars

b) The narrow HAZ (2.8 mm) and the shape of the flash formed in the FW of the steel bars

Figure 20

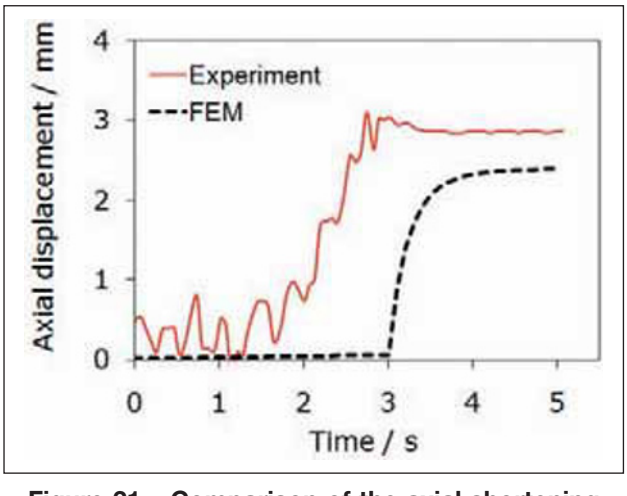

Figure 21 – Comparison of the axial shortening predicted by the FE model and that measured in the FW experiment

5.1.2 Verification of IHC assumptions

As indicated previously, to simplify the inverse analysis of the heat generation, the radiation and convection heat transfer to the environment were neglected and adiabatic boundary conditions were assumed. Moreover, in the deforming zone next to the friction surface, the heat generation rate owing to the plastic deformation $\dot{S}$ was also neglected as explained earlier. Since the heat input calculated by the IHC method is used for the FE analysis, these simplifications should therefore be verified.

Using the maximum effective stress and strain rate calculated with the FE model, the maximum heat generation rate due to plastic deformation (i.e., $\dot{S}$) is obtained with 30 W. On the other hand, using the area below the heat generation rate diagram calculated with the inverse method (Figure 17), the total frictional heat input is obtained with 24 kW. It follows that the amount of heat generated by deformation next to the friction interface zone is only about 0.1 % of the overall heat input by friction. Thus, it is reasonable to neglect the term $\dot{S}$ as assumed in the inverse model.

The validity of the thermal boundary conditions, i.e. insignificant heat loss to the environment and uniform temperature profile across the planes parallel to the friction interface, is confirmed by comparison of the temperature profiles between two points at the surface (P1) and the centre (P2) of a cross-section parallel and close (x = 1 mm) to the friction interface. The two points are illustrated in Figure 20 a) and the FE-calculated temperature profile is shown in Figure 22. The two temperature profiles are very close together and the maximum difference is almost negligible. This implies that the temperature distributions at cross-sections parallel to the heat source during the orbital friction welding cycle are homogenous and therefore, it is reasonable to assume that the lateral surfaces can be described with adiabatic boundary conditions.

5.2 Thermal-phase transformation model

During the FW process, the HAZ experiences a temperature change and is subject to a number of

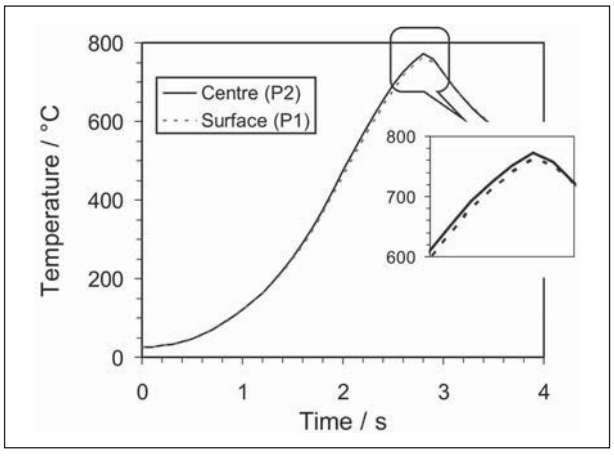

Location of the points P1 and P2 are shown in Figure 20 a).

Figure 22 – Comparison of temperature profiles between centre (P1) and surface (P2) of a cross-section close (x = 1 mm) and parallel to the friction surface calculated from FE analysis

microstructural transformations. The type and volume fraction of the final microstructure constituents, which are a function of welding peak temperature and subsequent cooling rate, will determine the weld properties, e.g., hardness, strength and ductility. In this part, a thermo-metallurgical FE model is developed, to predict the size of the heat-affected zone (HAZ) and the final microstructure of the weld.

The boundary conditions for the thermo-metallurgical FE model are similar to the thermo-mechanical model, however, thrust load and deformation are not considered in the latter. Therefore, the two rigid planes (see Figure 19) are removed for the simulation.

The calculation of reconstructive phase transformations in the DEFORM package is based on the experimental data stored in the form of isothermal transformation diagrams. The start of transformation under non-isothermal conditions (e.g. in FW) is predicted by Scheil's additivity rule [40]. The experimental kinetics data are fitted using the Kolmogorov-Johnson-Mehl-Avrami equation [40-41]. For the present model, the isothermal transformation diagram of the steel is implemented into the model [18]. The martensitic transformation is modelled using the Magee equation [42]. Based on the inverse heat input data and the microstructure evolution models, the volume fraction of all of the microstructure constituents across the weld and HAZ are calculated.

Figure 23 illustrates the distribution of pearlite after friction welding and cooling. The width of the HAZ is predicted to be 2.8 mm, which is in good agreement with the measured data shown in Figure 20 b). This agreement is expected, because an accurate temperature profile (see Figure 18) calculated by the inverse model has been used in the FE model. Therefore, if the time-temperature history of the orbital friction welding is accurately calculated, then the thermal phase transformation model can successfully predict the HAZ size and microstructure evolution of the weld.

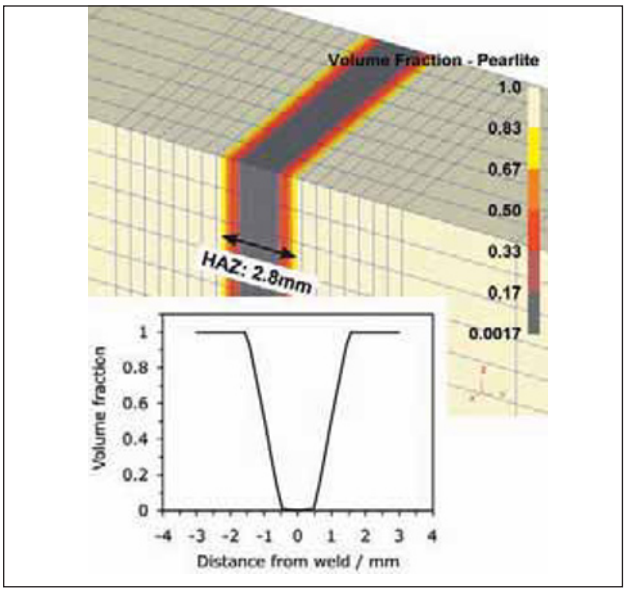

Predicted phase transformation region limits the width of the HAZ.

Figure 23 – Predicted volume fraction profile of pearlite after the orbital friction welding and cooling of the steel

6 SUMMARY

The orbital friction welding of eutectoid steel bars was investigated extensively and various features associated with the process such as heat generation, flash formation, microstructure evolution and phase transformation were studied.

It was experimentally observed that the insufficient frictional heat imposed on the weld interface leads to localized junctions in the rubbing interface. By using high-speed camera observation and increasing the dissipated heat at the rubbing surface, proper welding parameters could be obtained.

The effects of peak temperature and hot plastic deformation of austenite on welding, continuous cooling transformation diagram (WCCT) and the kinetics of pearlite and martensite were studied. It was shown that the plastic deformation of austenite arising during friction welding accelerates the pearlitic transformation, whereas the martensite transformation is retarded as a result of a mechanical stabilization phenomenon. The change in martensite start temperature was estimated quantitatively using the theory of mechanical stabilization.

It is demonstrated that the modelling of heat generation is crucial and critical for the thermal, mechanical and metallurgical analyses of the FW. One of the most important aspects of FW modelling is the prediction of the effects of the FW process parameters on the quality of the weld. An inverse heat conduction analysis (IHC) was proposed by which the friction heat generation was estimated. The present IHC model is an improvement over thermal models, in the sense that it captures the exact temperature profile by providing accurate heat generation values. The model itself is simple and more interesting is the fact that essential data such as friction coefficient and shear yield stress, as a function of temperature and other parameters, are not required as input data for the model. The applicability of the proposed IHC model can be extended by performing a few FW experiments with different welding parameters and calculating the heat generation for each experiment. Eventually, a relationship between the welding parameters and the heat generation terms can be established. This, in turn, can be used for further prediction of the effect of the welding parameters on the joint quality. Moreover, with this methodology, it would be possible to provide an inter-relationship between the apparent coefficients of friction, welding parameters and temperature. This will eventually eliminate the need for performing a weld in order to provide input data for modelling and the predictive capability of the model would thus be increased.

Based on the estimated heat input obtained from the IHC analysis, two FE models were carried out. First, in the coupled thermo-mechanical model, the thermal history, flash formation and axial shortening were successfully analyzed. Then, with the thermal phase transformation FE analysis, the final microstructure constituents after welding and the size of the HAZ were predicted. The proposed FE model is suitable for the optimization of the FW process parameters and pre- and post-weld heat treatment.

The models developed in this work can be used as tools for the future development and optimization of friction welding processes of different cross-sections and materials. By applying these models, a dramatic reduction in development time and costs can be expected.

ACKNOWLEDGEMENTS

This work was carried out at the Institute of Materials Science and Welding, Graz University of Technology, Austria. The financial support for this work as part of K–net JOIN, granted by the Austrian Federal Ministry of Economy and Labour, is gratefully acknowledged. The author would also like to thank Prof. H. Cerjak of Graz University of Technology, Austria, Prof. E. Kozeschnik of Vienna University of Technology, Austria, and Prof. H.K.D.H Bhadeshia of the University of Cambridge, United Kingdom, for their support, enthusiasm and fruitful discussions.

REFERENCES

[1] Maalekian M.: Friction welding - A critical assessment of literature, Science and Technology of Welding and Joining, 2007, vol. 12, 8, pp. 738-759.

[2] Maalekian M.: Friction welding of high carbon steel in large cross-section, PhD thesis, Graz University of Technology, Austria, 2007.

[3] Rykalin N.N., Pugin A.I., Vasil'eva V.A.: The heating and cooling of rods butt welded by the friction process, Svarochnoe Proizvodstvo (Welding Production), 1959, pp. 42-52.

[4] Vill V.I.: Energy distribution in friction welding of steel bars, Welding Production, Oct. 1959, pp. 31-41.

[5] Cheng C.J.: Transient temperature distribution during friction welding of two similar materials in tubular form, Welding Journal, 1962, vol. 41, 12, pp. 542-550.

[6] Wang K.K., Nagappan P.: Transient temperature distribution in inertia welding of steels, Welding Research Supplement, Sept. 1970, pp. 419s-426s.

[7] Rich T., Roberts R.: Thermal analysis for basic friction welding, Metal Construction and British Welding Journal, March 1971, pp. 93-98.

[8] Craine R.E., Francis A.: Frictional heat generated in the early stages of an orbital friction welding process, Wear, 1987, 114, pp. 355-365.

[9] Sluzalec A.: Thermal effects in friction welding, International Journal of Mechanical Sciences, 1990, vol. 32, no. 6, pp. 467-478.

[10] Midling O.T., Grong Ø.: A process model for friction welding of Al-Mg-Si alloys and Al-SiC metal matrix composites-I,HAZ temperature and strain rate distribution, Acta Metallurgica et Materialia, 1994, vol. 42, no. 5, pp. 1595-1609.

[11] Moa A. l, Massoni E.: Finite element simulation of the inertia welding of two similar parts, Engineering Computation, 1995, vol. 12, pp. 479-512.

[12] Bendzsak G.J., North T.H., Li Z.: Numerical model for steady-state flow in friction welding, Acta Materialia, 1997, vol. 45, no. 4, pp. 1735-1745.

[13] Balasubramanian V., Li Y., Stotler T., Crompton J., Soboyejo A., Katsube N., Soboyejo W.: A new frictional law for the modelling of continuous drive friction welding: application to 1045 steel welds, Materials and Manufacturing Processes, 1999, vol. 14, no. 6, pp. 845-860.

[14] Vairis A., Frost M.: Modelling the linear friction welding of titanium blocks, Materials Science and Engineering, 2000, A292, pp. 8-17.

[15] Dave V.R., Cola M.J., Hussen G.N.A.: Heat generation in the inertia welding of dissimilar tubes, Welding Research Supplement, Oct. 2001, pp. 246s-252s.

[16] Nguyen T.C., Weckman D.C.: A thermal and microstructure evolution model of direct-drive friction welding of plain carbon steel, Metallurgical and Materials Transactions, 2006, Vol. 37B, pp. 275-292.

[17] Maalekian M., Kozeschnik E., Brantner H.P., Cerjak H.: Inverse modelling and simulation of heat generation in friction welding, Mathematical modelling of weld phenomena 8, Editors: H. Cerjak, H.K.D.B. Bhadeshia, E. Kozeschnik (Eds.), Verlag der Technischen Universität Graz, 2007, pp. 881-890.

[18] Maalekian M., Kozeschnik E., Brantner H.P., Cerjak H.: Finite element modelling of orbital friction welding of eutectoid steel bars, Metallurgical and Materials Transactions, 2008, 39A, pp. 844-852.

[19] Maalekian M., Kozeschnik E., Brantner H.P., Cerjak H.: Comparative analysis of heat generation in friction welding of steels bars, Acta Materialia, 2008, 56, pp. 2843-2855.

[20] Maalekian M.: Thermal modeling of friction welding, ISIJ International, 2008, 48, pp. 1429-1433.

[21] Maalekian M., Cerjak H.: Thermal-phase transformation modelling and neural network analysis of friction welding of non-circular eutectoid steel components, Doc. IIW-1945-08 (ex-doc. IX-2275r1-08), Welding in the World, 2009, vol. 53, no. 3/4, pp. R44-R51.

[22] Orlich J., Pietrzeniuk H.J.: Atlas zur Wärmebehandlung der Stähle (Atlas of heat treatment of steels), Band 4, Verlag Stahleisen mbH, Düsseldorf, 1976.

[23] Maalekian M., Kozeschnik E., Chatterjee S., Bhadeshia H.K.D.H.: Mechanical stabilisation of eutectoid steel, Materials Science and Technology, 2007, vol. 23, no. 5, pp. 610-612.

[24] Chatterjee S., Wang H.S., Yang J.R., Bhadeshia H.K.D.H., Mechanical stabilisation of austenite, Materials Science and Technology, 2006, vol. 22, pp. 641–644.

[25] Khlestov V.M., Konopleva E.V., McQueen H.J.: Kinetics of austenite transformation during thermomechanical

processes, Canadian Metallurgical Quarterly, 1998, vol. 37, no. 2, pp. 75-89.

[26] Jandova D., Meyer L.W., Masek B., Novy Z., Kesner D., Motycka P.: The influence of thermo-mechanical processing on the microstructure of steel 20MoCrS4, Materials Science and Engineering, 2003, A349, pp. 36-47.

[27] Maalekian M., Lendinez M.L., Kozeschnik E., Brantner H.P., Cerjak H.: The influence of peak temperature and deformation on welding CCT diagram of eutectoid carbon steel, Advanced Materials Research, 2007, vol. 15-17, pp. 1008-1013.

[28] Maalekian M., Lendinez M.L., Kozeschnik E., Brantner H.P., Cerjak H.: Effect of hot plastic deformation of austenite on the transformation characteristics of eutectoid carbon steel under fast heating and cooling conditions, Materials Science and Engineering: A, 2007, vol. 454-455, pp. 446-452.

[29] Maalekian M., Kozeschnik E., Brantner H.P., Cerjak H.: On the influence of hot straining of austenite in solid-state welding of high carbon steel, Welding in the World, 2008, vol. 52, no. 1/2, Research Supplement, pp. 100-106.

[30] Imbert C.A.C., McQueen H.J.: Dynamic recrystalization of D2 and W1 tool steels, Materials Science and Technology, 2000, vol. 16, pp. 532-538.

[31] MTDATA, Software, National Physical Laboratory, Teddington, U.K., 2006.

[32] Gel'man A.S.: The nature of friction welding, Avt. Svarka, 1965, no. 3, pp. 5-10.

[33] Gel´man A.S., Sander M.P.: Power and heating in the friction welding of thick-walled steel pipes, Welding Production, Oct. 1959, pp. 53-61.

[34] Hollander M.B., Cheng C.J., Wyman J.C.: Friction welding parameter analysis, Welding Journal Research Supplement, Nov. 1963, pp. 495s-501s.

[35] Craine R.E., Francis A.: Frictional heat generated in the early stages of an orbital friction welding process, Wear, 1987, vol. 114, pp. 355-365.

[36] Midling O.T., Grong Ø.: A process model for friction welding of Al-Mg-Si alloys and Al-SiC metal matrix composites-II. HAZ microstructure and strength evolution, Acta Metallurgica et Materialia, 1994, vol. 42, no. 5, pp. 1611-1622.

[37] Hollander M.B.: Developments in friction welding, Metals Engineering Quarterly, May 1962, pp. 14-24.

[38] Scientific Forming Technologies Corporation, http://www.deform.com.

[39] Hosford W.F., Caddel R.M.: Metal forming: mechanics and metallurgy, Prentice-Hall, Inc., Englewood liffs, 1983.

[40] Bhadeshia H.K.D.H.: Bainite in steels, 2nd ed., The Institute of Materials, London, UK, 2001.

[41] Johnson W.A., Mehl R.H., Reaction kinetics in processes of nucleation and Growth, Trans. AIME, 1939, vol. 135, pp. 416-433.

[42] Magee C.L.: Phase Transformations, ASM, Metals Park, Ohio (1), 1970, pp. 15-156.